

Anomalous Electromagnetic Induction Engendered by Singular Gauge Transformation

Wei Luo,¹ Wei Chen,^{1,*} and D. Y. Xing¹

¹*National Laboratory of Solid State Microstructures, School of Physics,
and Collaborative Innovation Center of Advanced Microstructures, Nanjing University, Nanjing 210093, China*
(Dated: December 1, 2023)

The Berry curvature, resembling the magnetic field in reciprocal space, offers a captivating avenue for exploring unique electromagnetic phenomena devoid of real-space analogs. Here, we investigate the emergent electromagnetic induction by solenoidal Berry curvature with its field lines forming loops, links, and knots. In stark contrast to Faraday's law, which dictates that alternating magnetic fields yield alternating electric fields with a net zero average, the alternating Berry curvature can engender directional electromagnetic induction. Such an effect is attributed to the presence of singularities in the Berry curvature, accompanied by a 2π jump in the Berry flux. Notably, this jump does not trigger a diamagnetic impulse, due to the gauge invariance of the Berry phase modulo 2π . Consequently, the induced electric field maintains finite values under time averaging, manifesting itself as a directional pumping current. Our research sheds light on an anomalous electromagnetic induction effect directly arising from the singular gauge transformation, thereby expanding our comprehension of exotic electromagnetic phenomena.

The Berry phase effect has become an important research field in modern physics [1, 2], akin to the generalized Aharonov-Bohm phase [3] in parametric spaces. In solid-state physics, the Berry phase of the Bloch wave function accrues along closed trajectories in reciprocal space. Interestingly, physical properties such as the semiclassical dynamics of the Bloch electrons exhibit captivating duality between real and reciprocal spaces [4, 5], thereby offering a tangible perspective for understanding the topological properties in reciprocal space. Specifically, one can envision the Berry curvature as a local magnetic field in reciprocal space, imparting a wealth of intriguing characteristics to Bloch electrons [2]. Drawing inspiration from this analogy, novel effects traditionally confined to real space have recently found their implementation in reciprocal space. Noteworthy examples include the Aharonov-Bohm effect [6, 7] and Hall drift [8].

In addition to the physical effects that have counterparts in real space, there are also electromagnetic phenomena that are exclusive to reciprocal space. A prime example is the existence of magnetic monopoles in the reciprocal space of Weyl semimetals, serving as sources or drains for the Berry curvature [9, 10], while the corresponding object in real space remains elusive despite extensive pursuit. Mathematically, incorporating the effects of magnetic monopoles into the modified Maxwell equations is straightforward [11]. As a direct physical consequence, these Berry curvature monopoles can lead to anomalous electromagnetic induction (EMI) and resultant charge-pumping effects in Weyl semimetals [12–14]. In this context, an interesting question that arises is whether there are exotic emergent electromagnetic phenomena in reciprocal space that extend beyond the framework of Maxwell's theory.

In this work, we affirmatively answer this question by incorporating singularities in the theory of electrodynamics. Specifically, we investigate the emergent electro-

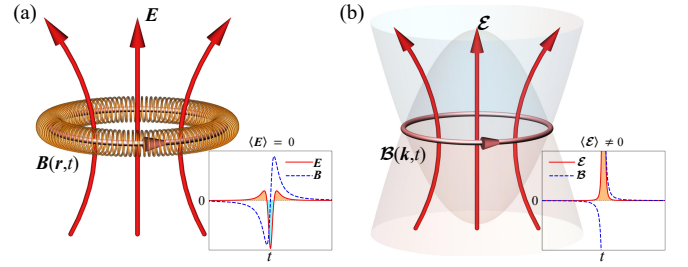


FIG. 1. (a) Schematic illustration of conventional electromagnetic induction: an alternating solenoidal magnetic field $\mathbf{B}(\mathbf{r}, t)$ induces an alternating electric field $\mathbf{E}(\mathbf{r}, t)$ with a zero time-averaged value. An abrupt change in $\mathbf{B}(\mathbf{r}, t)$ results in a strong diamagnetic impulse, as shown in the inset. (b) Anomalous electromagnetic induction: the induction of an emergent electric field $\mathcal{E}(\mathbf{k}, t)$ by solenoidal Berry curvature $\mathcal{B}(\mathbf{k}, t)$ with finite distributions around band crossing regions. Importantly, an abrupt change in the Berry flux by 2π does not lead to a diamagnetic electric impulse, resulting in non-zero average values of $\mathcal{E}(\mathbf{k}, t)$.

magnetic induction (EMI) generated by the time-varying solenoidal (divergence-free) Berry curvature $\mathcal{B}(\mathbf{k}, t)$, as illustrated in Fig. 1(b). It can be proved that the emergent electric field $\mathcal{E}(\mathbf{k}, t)$ and $\mathcal{B}(\mathbf{k}, t)$ satisfy the conventional Faraday's law of EMI, expressed as $\nabla_{\mathbf{k}} \times \mathcal{E} = -\partial \mathcal{B} / \partial t$. One might initially expect that a periodically variation of the Berry curvature would induce an alternating \mathcal{E} field with a zero time-averaged value, as its real-space counterpart shown in Fig. 1(a). However, this conclusion holds true only when the Berry curvature \mathcal{B} varies continuously with time, a characteristic inherent in a real magnetic field \mathbf{B} but not in \mathcal{B} . Notably, the Berry curvature $\mathcal{B}(\mathbf{k}, t)$ in reciprocal space can accommodate singularities and abrupt changes in its flux by multiples of 2π . Given that the Berry phase is gauge-invariant modulo 2π , abrupt shifts in the Berry flux from $-\pi$ to

π do not induce diamagnetic electric impulses, as seen in the comparison between the insets in Figs. 1(a) and 1(b). Consequently, due to the absence of such counteractive impulses, the \mathcal{E} field possesses a finite value under time averaging, which can be probed through the charge pumping effect. Based on this argument, it becomes apparent that this directional EMI induced by alternating solenoidal Berry curvature is a direct manifestation of the singular gauge transformation (SGT). Furthermore, we extend our investigation to explore the emergent EMI effect induced by other solenoidal Berry curvature with its field lines forming links and knots, thereby enriching the resultant topological pumping effect. Our theory unveils an anomalous electromagnetic phenomenon in reciprocal space, devoid of any real-space counterparts.

An elementary example of solenoidal Berry curvature can be realized through a linear band crossing, as shown in Fig. 1(b), accompanied by a mass term. This system is described by the Hamiltonian given as

$$H(\mathbf{k}, t) = \lambda k_z \sigma_x + g_y(t) \sigma_y + [\eta(k_0^2 - k^2) + g_z(t)] \sigma_z, \quad (1)$$

where $k = \sqrt{k_x^2 + k_y^2 + k_z^2}$ is the magnitude of the momentum, the Pauli matrices $\sigma_{x,y,z}$ act on the (pseudo-)spin, λ and η are model parameters. The two driving terms $g_y(t) = g_1 \sin(\omega t)$ and $g_z(t) = g_2 \cos(\omega t)$ introduce periodic modulations to the Berry curvature, leading to the EMI effect. The instantaneous eigenvalues of the Hamiltonian are $\varepsilon_\alpha(\mathbf{k}, t) = \alpha \sqrt{\lambda^2 k_z^2 + g_y(t)^2 + [\eta(k_0^2 - k^2) + g_z(t)]^2}$, with corresponding eigenstates represented as $|\chi_\alpha(\mathbf{k}, t)\rangle$, where $\alpha = \pm$ denotes the conduction and valence bands. We assume $g_2 > \eta k_0^2$ to ensure that the two bands periodically intersect at $t = 2n\pi/\omega$ along the circular nodal loop, denoted by C_0 , having a radius $k_1 = k_0[1 + g_2/(\eta k_0^2)]^{1/2}$ in the $k_z = 0$ plane, as depicted in Fig. 2(a). The time-dependent Berry curvature under the valence band is calculated by $\mathcal{B}(\mathbf{k}, t) = \nabla_{\mathbf{k}} \times \mathcal{A}$ with $\mathcal{A} = i\langle \chi_- | \nabla_{\mathbf{k}} | \chi_- \rangle$ the Berry connection, which yields

$$\mathcal{B}(\mathbf{k}, t) = \lambda \eta (k_x^2 + k_y^2)^{1/2} g_1 \sin(\omega t) \hat{e}_\theta / \varepsilon_+^3. \quad (2)$$

Note that \mathcal{B} possesses only the azimuth component with its direction indicated by the unit vector \hat{e}_θ . Moreover, it converges into divergent $\pm\pi$ Berry fluxes along the nodal loop at $t = 2n\pi/\omega \pm 0^+$ for any integer n .

We solve the time evolution of the wave function to investigate the physical effect induced by the variation of the Berry curvature. Without loss of generality, we consider an initial state $|\chi_-(\mathbf{k}, 0)\rangle$ in the valence band, which evolves into $|\psi_-(t)\rangle = |\chi_-(t)\rangle - i\hbar \frac{\langle \chi_+ | \partial_t \chi_+ \rangle}{\varepsilon_- - \varepsilon_+} |\chi_+(t)\rangle$ to first-order approximation. This evolution arises from the gradual changes in both the momentum \mathbf{k} and the driving terms $g_{y,z}(t)$. The time derivative in the second term is explicitly expressed as $|\partial_t \chi_\alpha\rangle = \dot{\mathbf{k}} \cdot \nabla_{\mathbf{k}} |\chi_\alpha\rangle + \sum_{j=y,z} \dot{g}_j \partial_{g_j} |\chi_\alpha\rangle$. The average value of the velocity

$\dot{\mathbf{r}}(\mathbf{k}, t) = \nabla_{\mathbf{k}} H(\mathbf{k}, t)$ with respect to the state $|\psi_-(t)\rangle$ is obtained as [4]

$$\dot{\mathbf{r}} = \nabla_{\mathbf{k}} \varepsilon_- + \dot{\mathbf{k}} \times \mathcal{B} + \mathcal{E}, \quad (3)$$

where the last term is expressed as

$$\mathcal{E} = i \sum_{j=y,z} \dot{g}_j (\langle \nabla_{\mathbf{k}} \chi_- | \partial_{g_j} \chi_- \rangle - \langle \partial_{g_j} \chi_- | \nabla_{\mathbf{k}} \chi_- \rangle). \quad (4)$$

It can be decomposed into transverse and longitudinal components as $\mathcal{E} = \mathcal{E}^t + \mathcal{E}^l$. Eq. (3) takes on a similar form to its dual equation $\dot{\mathbf{k}} = \dot{\mathbf{r}} \times \mathcal{B} + \mathcal{E}$, which describes the momentum change of a charged particle (with unity charge) due to the electromagnetic fields \mathcal{B} and \mathcal{E} . By drawing this analogy, the Berry curvature \mathcal{B} resembles the magnetic field, while \mathcal{E} can be regarded as the emergent electric field in reciprocal space [12]. Interestingly, these fictitious fields in reciprocal space also adhere to Faraday's law, as can be confirmed by taking the curl on both sides of Eq. (4). Substituting $|\chi_- \rangle$ into Eq. (4), we obtain the three components of the \mathcal{E} field

$$\begin{aligned} \mathcal{E}_{x(y)} &= \lambda g_1 \omega \eta k_{x(y)} k_z \cos(\omega t) / \varepsilon_+^3, \\ \mathcal{E}_z &= \lambda g_1 \omega [g_2 + \eta(k_0^2 - k^2 + 2k_z^2) \cos(\omega t)] / (2\varepsilon_+^3). \end{aligned} \quad (5)$$

In Fig. 2(a), we illustrate the time-averaged distribution of $\mathcal{E}(\mathbf{k})$ in reciprocal space, resembling the electric field induced by the varying solenoidal magnetic field.

Here, the key result is that even though the Hamiltonian and the resultant Berry curvature \mathcal{B} exhibit periodic variations over time, the induced \mathcal{E} field and its transverse component \mathcal{E}^t maintain non-zero average values. This outcome stands in contrast to Faraday's law, which dictates that an alternating magnetic field generates an alternating electric field with an average value of zero. This underscores a clear differentiation between electromagnetic phenomena in reciprocal and real spaces. A crucial point is that the Berry curvature \mathcal{B} can harbor singularities. It is the SGT, characterized by an abrupt change in the Berry flux carried by the singular Berry curvature ($\Phi : -\pi \rightarrow \pi$), that leads to a finite average value of \mathcal{E} , a phenomenon absent in its real-space counterpart.

To illustrate this point, let us begin by focusing on the transverse field \mathcal{E}^t , which is solely induced by \mathcal{B} . Due to the rotational invariance of the system about the z axis, the distribution of \mathcal{B} can be broken down into various circular loops centered on the k_z axis, as depicted in Fig. 2(a). The variations of \mathcal{B} in these loops induce \mathcal{E}^t . For most of these circular loops, denoted by C_i , where no singularity in \mathcal{B} occurs during each driving cycle, the average value of \mathcal{E}^t is zero, following the Biot-Savart law $\langle \mathcal{E}^t(\mathbf{k}, C_i) \rangle = -\frac{\Delta \mathcal{B} \delta A}{T} \oint_{C_i} \frac{d\mathbf{k}' \times (\mathbf{k} - \mathbf{k}')}{|\mathbf{k} - \mathbf{k}'|^3} = 0$. Here, $d\mathbf{k}'$ is the vector element along C_i , $T = 2\pi/\omega$ is the driving period, and δA denotes the cross-sectional area of the tiny circular tube enclosing C_i . Since the magnitude of

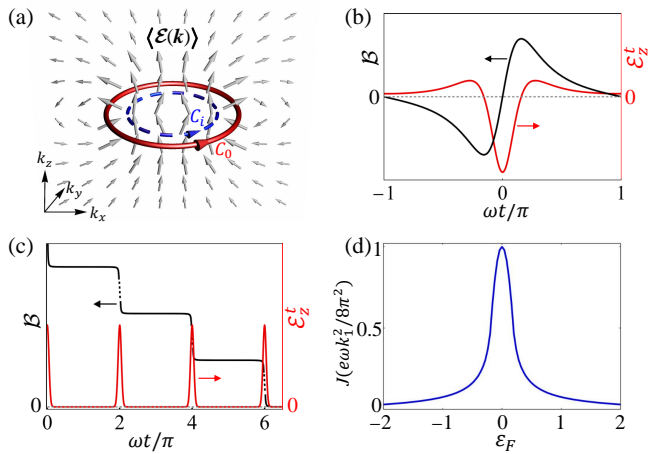


FIG. 2. (a) Illustration of the singular loop C_0 (red circle) and a regular loop C_i (blue circle), with arrows indicating the direction of the Berry curvature. The time-averaged distribution of the $\mathcal{E}(\mathbf{k})$ field is represented by the gray vectors. Only the distribution in the k_x - k_z plane is shown for clarity, and its entire distribution possesses rotational symmetry around the k_z axis. (b) Time dependence of the Berry curvature on the loop with radius $k_\rho = 0.85k_1$ lying in the $k_z = 0$ plane and the z component of the induced transverse electric field \mathcal{E}_z^t at the origin. (c) Time dependence of the Berry curvature on the red loop C_0 after singular gauge transformation and the induced \mathcal{E}_z^t at the origin. (d) Pumping current density as a function of the Fermi energy ε_F . The parameters are set to $g_1 = 2$, $g_2 = 2$, $k_0 = 1.3$, $\lambda = 1$, and $\eta = 1$.

the Berry curvature \mathcal{B} is a regular function of time, its variation within one period is zero, i.e., $\Delta\mathcal{B} = 0$. This results in $\langle \mathcal{E}^t(\mathbf{k}, C_i) \rangle = 0$, which can be confirmed by Fig. 2(b).

In contrast to the C_i loops, \mathcal{B} exhibits periodic divergence along the C_0 loop and undergoes an abrupt change in its Berry flux by 2π . Given that the Berry phase is gauge-invariant modulo 2π , the $\pm\pi$ Berry fluxes are essentially equivalent. Leveraging this property, we can re-express the periodically varying Berry curvature along the C_0 loop as follows

$$\tilde{\mathcal{B}}_0(\mathbf{k}, t) \equiv \mathcal{B}_0(\mathbf{k}, t) - \left[\sum_{n=1}^{\infty} \Theta(t - nT) \right] \delta\mathcal{B}(\mathbf{k}) \hat{e}_\theta, \quad (6)$$

where $\delta\mathcal{B}(\mathbf{k}) = 2\pi\delta(k_z)\delta[k_1 - (k_x^2 + k_y^2)^{1/2}]$ captures the change in Berry flux and Θ is the unit step function. This SGT effectively converts the periodic function into a continuous, monotonically decreasing function characterized by a series of steps, as shown in Fig. 2(c). Each jump of $\tilde{\mathcal{B}}_0$ induces an identical pulse in \mathcal{E}^t . Therefore, it is the SGT that enables directional EMI by the alternating Berry curvature.

The directional EMI induced by the SGT can be manifested as charge pumping driven by the emergent field \mathcal{E} . We first consider a fully occupied valence band. The

average current density, denoted as \mathbf{J} , can be obtained by integrating the velocity $\dot{\mathbf{r}}(\mathbf{k}, t)$ across the entire band, which simplifies to

$$\mathbf{J} = \frac{e}{T} \int_0^T dt \int \frac{d^3\mathbf{k}}{(2\pi)^3} \mathcal{E}(\mathbf{k}, t). \quad (7)$$

It is worth noting that the contributions from the first two terms in Eq. (3) both vanish after integration. This implies that the current density is directly proportional to the average \mathcal{E} field in reciprocal space. Inserting Eq. (5) into Eq. (7) yields

$$\mathbf{J} = \frac{e\omega}{8\pi^2} k_1^2 \hat{z}. \quad (8)$$

Here, the current flows in the z direction since only \mathcal{E}_z has a nonzero average value. This result can be understood straightforwardly by breaking down the 3D system into multiple 1D channels in reciprocal space, with each channel labeled by (k_x, k_y) and oriented in the z direction. Eq. (8) implies that each 1D channel within the nodal loop with $k_\rho = \sqrt{k_x^2 + k_y^2} < k_1$ makes an equal contribution to the current. This result aligns with the characteristics of $\langle \mathcal{E}(\mathbf{k}) \rangle$ presented in Fig. 2(a): \mathcal{E}_z maintains consistently positive as k_z varies for $k_\rho < k_1$, whereas it changes sign as k_z varies for $k_\rho > k_1$, ultimately resulting in an average value of zero. To be precise, when we perform partial integration of $\frac{1}{2\pi} \int dk_z dt \mathcal{E}_z$ in Eq. (7), we obtain a Chern number of 1 for $k_\rho < k_1$ and a Chern number of 0 for $k_\rho > k_1$.

In more general scenarios, the electron bands are only partially occupied. For instance, we consider the valence band initially ($t = 0$) filled up to a certain negative energy level $\varepsilon_F < 0$. Additionally, we focus on the adiabatic regime where the electron occupation remains constant during the time evolution. This requirement implies that the pumping frequency ω is much higher than the inverse relaxation time $1/\tau$. Under these conditions, the pumping current can still be calculated using Eq. (7), with the integration now performed over the occupied states rather than the entire band. Similarly, for a positive Fermi energy $\varepsilon_F > 0$, the contribution from the conduction band should also be taken into account. However, in both of these partially occupied scenarios, no quantized expression like Eq. (8) is available and so we present the numerical results in Fig. 2(d). It shows that the pumping current decreases as the Fermi distribution deviates from the fully occupied state of the valence band. The symmetrical structure around zero energy signifies that both the energy levels and the emergent \mathcal{E} field have opposite signs for the two bands.

It is straightforward to extend the EMI effect to more complex configurations of the solenoidal Berry curvature, such as links and knots. These novel field configurations have been explored in various contexts, including electromagnetic fields [15–23]. Correspondingly, similar objects

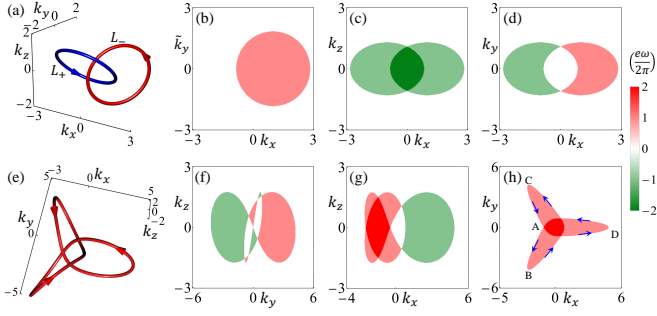


FIG. 3. (a) Berry curvature with a Hopf link structure. The distribution of the pumping current density in (b) \hat{n}_+ , (c) y , and (d) z directions in the corresponding projected reciprocal spaces. (e) Berry curvature with a knot structure. The distribution of the pumping current density in (f) x , (g) y , and (h) z directions. The parameters are set to $g_1 = g_2 = 1$, and (a-d) $m_0 = 0.2$, (e-h) $m_0 = 0.1$.

associated with the Berry curvature in reciprocal space have also been proposed [24–26]. To investigate the EMI caused by the solenoidal Berry curvature forming a Hopf link, we employ the following Hamiltonian

$$H_{\text{link}}(\mathbf{k}, t) = [2k_x k_z + 2k_y m(t)] \sigma_x + g_y(t) \sigma_y + [k_x^2 + k_y^2 - k_z^2 - m^2(t)] \sigma_z, \quad (9)$$

where we set all coefficients to unity for simplicity, and $m(t) = m_0 + g_z(t) - k^2/2$. We assume that $g_2 > m_0 + 1/2$ to ensure that the conduction and valence bands periodically intersect at $t = 2n\pi/\omega$ along two linked nodal loops. These loops are defined by parametric equations: $k_y = k_z$, $(k_x - 1)^2 + k_y^2 + k_z^2 = 2(m_0 + g_2) + 1$ for one loop, and $k_y = -k_z$, $(k_x + 1)^2 + k_y^2 + k_z^2 = 2(m_0 + g_2) + 1$ for the other; see Fig. 3(a).

Similar to the situation with a single loop, the Berry curvature exhibits divergence along the linked nodal loops at $t = 2n\pi/\omega$. The occurrence of this singularity is accompanied by a 2π jump in the Berry flux, which induces an \mathcal{E} field for each loop in the respective direction. Specifically, the two nodal loops L_{\pm} , situated in the planes $k_y = \pm k_z$ as depicted Fig. 3(a), generate average pumping currents in the directions $\hat{n}_{\pm} = (0, -1, \pm 1)$, which are perpendicular to the corresponding planes. The total current is a joint contribution from both nodal loops. We consider a fully occupied valence band and calculate the pumping current in the \hat{n}_+ direction. In this case, only the L_+ loop, with its plane perpendicular to \hat{n}_+ , contributes to the current. It is insightful to examine the current distribution in each channel labelled by (k_x, \tilde{k}_y) , where $\tilde{k}_y = (k_y + k_z)/\sqrt{2}$; see Fig. 3(b). One can see that each 1D channel within the nodal loop contributes a current density of $e\omega/(2\pi)$. Consequently, the total current density is given by $\mathbf{J} = e\omega S/(8\pi^3) \hat{n}_+$ with $S = \pi[2(m_0 + g_z) + 1]$ representing the area encircled by L_+ , consistent with the findings for a single nodal loop.

Similarly, one can derive the current distribution in the \hat{n}_- direction, which is solely induced by the nodal loop L_- .

In a general direction, the pumping current contains the contribution from both nodal loops, L_{\pm} . The channel-resolved current density distributions in the y and z directions are shown in Figs. 3(c,d). Within the projection area encircled by the linked nodal loops, the current density is quantized for each channel. In Figs. 3(c,d), there are two types of regions where the projections of the two loops either overlap or do not. In the non-overlapping region, the current density is $\pm e\omega/(2\pi)$ for each channel with its sign determined by the direction of the \mathcal{E} field induced by the corresponding nodal loop. In the overlapping region, the pumping current in each channel consists of the contributions from both loops: it doubles due to the same direction of the currents induced by the two loops in Fig. 3(c), whereas the currents induced by the two nodal loops cancel each other out in Fig. 3(d). The total pumping current is obtained by integrating the contributions from all channels. In the y direction, the total current density is $J_y = -e\omega S_1/(4\pi^3)$, where $S_1 = S/\sqrt{2}$ represents the projected area of one nodal loop. By contrast, the current density in the z direction is zero because the currents induced by the two loops are opposite in sign. Moreover, the current in the x direction also vanishes simply because the projection of both loops does not enclose any area.

The EMI by the varying Berry curvature forming a knot structure can be described by the following model

$$H_{\text{knot}}(\mathbf{k}, t) = [k_x^3 - 3k_x k_y^2 + k_z^2 - m^2(t)] \sigma_x + g_y(t) \sigma_y + [3k_x^2 k_y - k_y^3 + 2k_z m(t)] \sigma_z. \quad (10)$$

Again, the SGT plays a central role in the topological pumping effect. At $t = 2n\pi/\omega$, band degeneracy occurs periodically along the nodal loop that forms a knot as shown in Fig. 3(e). This is accompanied by a 2π jump in the Berry flux. We calculate the distribution of the pumping current density along the x , y , and z directions; see Figs. 3(f-h). One can see that the regions exhibiting nontrivial current distributions are encircled by the projection of the nodal knot. The rich structure of the current distributions reveals the complex configurations of a knot. The pumping current associated with a specific momentum channel is determined by multiplying $e\omega/(2\pi)$ by the winding number, which is calculated by tracing the projection of the arrowed nodal knot in the plane surrounding the reference momentum point. Using Fig. 3(h) as an example, the projected nodal knot follows the path denoted by the blue arrows, *ABACADA*. In the central region, the winding number is two, while in the three petal-shaped regions, it equals one. It can be confirmed that the distribution of pumping current in different directions follows the same rule when meticulously tracking the projected trajectory of the nodal

knot. Moreover, the interpretation of pumping current through the winding number holds true for all examples presented in this study. In the case of the nodal link, the total winding number is the sum of those defined by the two individual loops.

The anomalous EMI effect can be hopefully implemented in nodal-line semimetals [27–39] that possess both spin-orbit coupling and magnetic order. In such a scenario, the Pauli matrices in the Hamiltonian (1) represent the real electronic spin. The nodal loop naturally carries a singular Berry flux of $\pm\pi$, which is the central ingredient for the anomalous EMI. Moreover, the driving terms $g_{y,z}(t)$ can be achieved by the precessing magnetization controlled by ferromagnetic resonance [40], a well-established technique in spin pumping [41, 42]. The EMI can then be probed by the pumping current driven by the microwave. Interestingly, recent advancements have led to the observation of nodal link semimetals in a magnetic material [43, 44], which opens the possibility for the implementation of anomalous EMI effect induced by solenoidal Berry curvature with link and knot configurations. Additionally, it is also of particular interest to explore such exotic electromagnetic phenomena in engineered systems such as ultracold atoms [45] and photonics [46].

This work was supported by the National Natural Science Foundation of China under Grant No. 12074172 (W.C.), No. 12222406 (W.C.), and No. 12264019 (W.L.), and the State Key Program for Basic Researches of China under Grants No. 2017YFA0303203 (D.Y.X.).

* Corresponding author: pchenweis@gmail.com

- [1] M. V. Berry, “Quantal phase factors accompanying adiabatic changes,” *Proc. R. Soc. London, Ser. A* **392**, 45 (1984).
- [2] D. Xiao, M.-C. Chang, and Q. Niu, “Berry phase effects on electronic properties,” *Rev. Mod. Phys.* **82**, 1959–2007 (2010).
- [3] Y. Aharonov and D. Bohm, “Significance of electromagnetic potentials in the quantum theory,” *Phys. Rev.* **115**, 485–491 (1959).
- [4] Swati Chaudhary, Manuel Endres, and Gil Refael, “Berry electrodynamics: Anomalous drift and pumping from a time-dependent berry connection,” *Phys. Rev. B* **98**, 064310 (2018).
- [5] Steven M Girvin and Kun Yang, *Modern condensed matter physics* (Cambridge University Press, 2019).
- [6] N. Flaschner, B. S. Rem, M. Tarnowski, D. Vogel, D.-S. Luhmann, K. Sengstock, and C. Weitenberg, “Experimental reconstruction of the Berry curvature in a Floquet bloch band,” *Science* **352**, 1091 (2016).
- [7] L. Duca, T. Li, M. Reitter, I. Bloch, M. Schleier-Smith, and U. Schneider, “An Aharonov-Bohm interferometer for determining bloch band topology,” *Science* **347**, 288 (2015).
- [8] G. Jotzu, M. Messer, R. Desbuquois, M. Lebrat, T. Uehlinger, D. Greif, and T. Esslinger, “Experimental realization of the topological haldane model with ultracold fermions,” *Nature* **515**, 237 (2014).
- [9] X. Wan, A. M. Turner, A. Vishwanath, and S. Y. Savrasov, “Topological semimetal and fermi-arc surface states in the electronic structure of pyrochlore iridates,” *Phys. Rev. B* **83**, 205101 (2011).
- [10] N. P. Armitage, E. J. Mele, and A. Vishwanath, “Weyl and dirac semimetals in three-dimensional solids,” *Rev. Mod. Phys.* **90**, 015001 (2018).
- [11] John David Jackson, *Classical electrodynamics* (American Association of Physics Teachers, 1999).
- [12] H. Ishizuka, T. Hayata, M. Ueda, and N. Nagaosa, “Emergent electromagnetic induction and adiabatic charge pumping in noncentrosymmetric Weyl semimetals,” *Phys. Rev. Lett.* **117**, 216601 (2016).
- [13] H. Ishizuka, T. Hayata, M. Ueda, and N. Nagaosa, “Momentum-space electromagnetic induction in Weyl semimetals,” *Phys. Rev. B* **95**, 245211 (2017).
- [14] Qiong Ma, Su-Yang Xu, Ching-Kit Chan, Cheng-Long Zhang, Guoqing Chang, Yuxuan Lin, Weiwei Xie, Tomás Palacios, Hsin Lin, Shuang Jia, *et al.*, “Direct optical detection of weyl fermion chirality in a topological semimetal,” *Nature Physics* **13**, 842–847 (2017).
- [15] Antonio F Ranada, “A topological theory of the electromagnetic field,” *Letters in Mathematical Physics* **18**, 97–106 (1989).
- [16] Antonio F Ranada, “Knotted solutions of the maxwell equations in vacuum,” *Journal of Physics A: Mathematical and General* **23**, L815 (1990).
- [17] AM Kamchatnov, “Topological solitons in magnetohydrodynamics,” *Zh. Eksp. Teor. Fiz* **82**, 117–124 (1982).
- [18] Antonio F Ranada and José L Trueba, “Ball lightning an electromagnetic knot?” *Nature* **383**, 32–32 (1996).
- [19] Ludvig Faddeev and Antti J Niemi, “Stable knot-like structures in classical field theory,” *Nature* **387**, 58–61 (1997).
- [20] Richard A. Battye and P. M. Sutcliffe, “Knots as stable soliton solutions in a three-dimensional classical field theory,” *Phys. Rev. Lett.* **81**, 4798–4801 (1998).
- [21] Eugen Radu and Mikhail S Volkov, “Stationary ring solitons in field theory knots and vortons,” *Physics Reports* **468**, 101–151 (2008).
- [22] Yuki Kawaguchi, Muneto Nitta, and Masahito Ueda, “Knots in a spinor bose-einstein condensate,” *Phys. Rev. Lett.* **100**, 180403 (2008).
- [23] David S Hall, Michael W Ray, Konstantin Tiurev, Emmi Ruokokoski, Andrei Horia Gheorghe, and Mikko Möttönen, “Tying quantum knots,” *Nature physics* **12**, 478–483 (2016).
- [24] W. Chen, H.-Z. Lu, and J.-M. Hou, “Topological semimetals with a double-helix nodal link,” *Phys. Rev. B* **96**, 041102 (2017).
- [25] Z. Yan, R. Bi, H. Shen, L. Lu, S.-C. Zhang, and Z. Wang, “Nodal-link semimetals,” *Phys. Rev. B* **96**, 041103 (2017).
- [26] Ren Bi, Zhongbo Yan, Ling Lu, and Zhong Wang, “Nodal-knot semimetals,” *Phys. Rev. B* **96**, 201305 (2017).
- [27] Y. Kim, B. J. Wieder, C. L. Kane, and A. M. Rappe, “Dirac line nodes in inversion-symmetric crystals,” *Phys. Rev. Lett.* **115**, 036806 (2015).
- [28] R. Yu, H. Weng, Z. Fang, X. Dai, and X. Hu, “Topological node-line semimetal and Dirac semimetal state in

- antiperovskite Cu_3PdN ,” *Phys. Rev. Lett.* **115**, 036807 (2015).
- [29] T. T. Heikkilä, N. B. Kopnin, and G. E. Volovik, “Flat bands in topological media,” *JETP Letters* **94**, 233 (2011).
- [30] H. Weng, Y. Liang, Q. Xu, R. Yu, Z. Fang, X. Dai, and Y. Kawazoe, “Topological node-line semimetal in three-dimensional graphene networks,” *Phys. Rev. B* **92**, 045108 (2015).
- [31] Yuanping Chen, Yuee Xie, Shengyuan A. Yang, Hui Pan, Fan Zhang, Marvin L. Cohen, and Shengbai Zhang, “Nanostructured carbon allotropes with weyl-like loops and points,” *Nano Letters* **15**, 6974–6978 (2015).
- [32] Minggang Zeng, Chen Fang, Guoqing Chang, Yu-An Chen, Timothy Hsieh, Arun Bansil, Hsin Lin, and Liang Fu, “Topological semimetals and topological insulators in rare earth monopnictides,” arXiv:1504.03492 [cond-mat] (2015), arXiv: 1504.03492.
- [33] C. Fang, Y. Chen, H.-Y. Kee, and L. Fu, “Topological nodal line semimetals with and without spin-orbital coupling,” *Phys. Rev. B* **92**, 081201 (2015).
- [34] Ai Yamakage, Youichi Yamakawa, Yukio Tanaka, and Yoshihiko Okamoto, “Line-node dirac semimetal and topological insulating phase in noncentrosymmetric pnictides CaAgX ($x = \text{p, as}$),” *Journal of the Physical Society of Japan* **85**, 013708 (2016).
- [35] Lilia S. Xie, Leslie M. Schoop, Elizabeth M. Seibel, Quinn D. Gibson, Weiwei Xie, and Robert J. Cava, “A new form of ca3p2 with a ring of dirac nodes,” *APL Materials* **3**, 083602 (2015).
- [36] Y.-H. Chan, C.-K. Chiu, M. Y. Chou, and A. P. Schnyder, “ Ca_3P_2 and other topological semimetals with line nodes and drumhead surface states,” *Phys. Rev. B* **93**, 205132 (2016).
- [37] J. Zhao, R. Yu, H. Weng, and Z. Fang, “Topological node-line semimetal in compressed black phosphorus,” *Phys. Rev. B* **94**, 195104 (2016).
- [38] Guang Bian, Tay-Rong Chang, Hao Zheng, Saavanth Velury, Su-Yang Xu, Titus Neupert, Ching-Kai Chiu, Shin-Ming Huang, Daniel S. Sanchez, Ilya Belopolski, Nasser Alidoust, Peng-Jen Chen, Guoqing Chang, Arun Bansil, Horng-Tay Jeng, Hsin Lin, and M. Zahid Hasan, “Drumhead surface states and topological nodal-line fermions in tltaSe_2 ,” *Phys. Rev. B* **93**, 121113 (2016).
- [39] Guang Bian, Tay-Rong Chang, Raman Sankar, Su-Yang Xu, Hao Zheng, Titus Neupert, Ching-Kai Chiu, Shin-Ming Huang, Guoqing Chang, Ilya Belopolski, Daniel S. Sanchez, Madhab Neupane, Nasser Alidoust, Chang Liu, BaoKai Wang, Chi-Cheng Lee, Horng-Tay Jeng, Chenglong Zhang, Zhujun Yuan, Shuang Jia, Arun Bansil, Fangcheng Chou, Hsin Lin, and M. Zahid Hasan, “Topological nodal-line fermions in spin-orbit metal PbTaSe_2 ,” *Nature Communications* **7**, 10556 (2016).
- [40] Charles Kittel, “On the theory of ferromagnetic resonance absorption,” *Phys. Rev.* **73**, 155–161 (1948).
- [41] Yaroslav Tserkovnyak, Arne Brataas, Gerrit E. W. Bauer, and Bertrand I. Halperin, “Nonlocal magnetization dynamics in ferromagnetic heterostructures,” *Rev. Mod. Phys.* **77**, 1375–1421 (2005).
- [42] Kazuya Ando, Saburo Takahashi, Junichi Ieda, Yosuke Kajiwara, Hiroyasu Nakayama, Tatsuro Yoshino, Kazuya Harii, Yasunori Fujikawa, M Matsuo, S Maekawa, *et al.*, “Inverse spin-hall effect induced by spin pumping in metallic system,” *Journal of applied physics* **109** (2011).
- [43] Ilya Belopolski, Guoqing Chang, Tyler A Cochran, Zi-Jia Cheng, Xian P Yang, Cole Hugelmeier, Kaustuv Manna, Jia-Xin Yin, Guangming Cheng, Daniel Multer, *et al.*, “Observation of a linked-loop quantum state in a topological magnet,” *Nature* **604**, 647–652 (2022).
- [44] Guoqing Chang, Su-Yang Xu, Xiaoting Zhou, Shin-Ming Huang, Bahadur Singh, Baokai Wang, Ilya Belopolski, Jiaxin Yin, Songtian Zhang, Arun Bansil, Hsin Lin, and M. Zahid Hasan, “Topological hopf and chain link semimetal states and their application to co_2MnGa ,” *Phys. Rev. Lett.* **119**, 156401 (2017).
- [45] Michael Lohse, Christian Schweizer, Hannah M Price, Oded Zilberberg, and Immanuel Bloch, “Exploring 4d quantum hall physics with a 2d topological charge pump,” *Nature* **553**, 55–58 (2018).
- [46] Oded Zilberberg, Sheng Huang, Jonathan Guglielmon, Mohan Wang, Kevin P Chen, Yaacov E Kraus, and Mikael C Rechtsman, “Photonic topological boundary pumping as a probe of 4d quantum hall physics,” *Nature* **553**, 59–62 (2018).